ISEIS

Journal of Environmental Informatics 34(2) 108-122 (2018)

Journal of Environmental Informatics

www.iseis.org/jei

Remote Sensing of Harmful Algal Blooms Variability for Lake Hulun Using Adjusted FAI (AFAI) Algorithm

C. Fang[1,2], K.S. Song[1], Y.X. Shang[1,2], J.H. Ma[1,2], Z.D. Wen[1] and J. Du[1]

[1]*Northeast Institute of Geography and Agroecology, Chinese Academy of Sciences, Changchun 130102, China*
[2]*University of Chinese Academy of Sciences, Beijing 100049, China*

Received 5 December 2016; revised 8 December 2017; accepted 23 December 2017; published online 06 December 2018

ABSTRACT. Harmful algal blooms (HABs) have become a global issue due to their serious threat to environmental ecology and rapid expansion around the world. Northeast China, characterized by a long ice period, has been ignored in the previous studies of HABs. However, Lake Hulun, a great lake located in Northeast China, has been found intense HABs since the 1980s. To evaluate HABs more precisely and efficiently through satellite images in Lake Hulun, an adjusted FAI (AFAI) method with an automatically identified threshold was developed. The method took full advantage of Landsat series sensors and MODIS products, and built a threshold selection range (0.01 ~ 0.02 for Landsat and 0.05 ~ 0.12 for MODIS) rather than a single threshold on all images. With the long-term satellite data from year 1983 to 2016, occurrences of HABs in Lake Hulun were investigated. There were total 169 occurrences of HABs during the periods and the first outbreak was detected in 1984. Though the initial outbreak date of HABs varied in each year, most HABs happened in July and August. The water quality of Lake Hulun have experienced a serious degradation especially in the past nine years as the outbreak frequency of HABs increased a lot since 2009. The reason of the degradation may be attributed to the continuous grazing around the lake, tourism, and anthropogenic activities on lake surface even in freezing period. Surrounding land use and land cover (LUCC), meteorological conditions, and water chemical and physical parameters were also related with the outbreak of HABs to some extent.

Keywords: AFAI, HABs, Lake Hulun, Landsat, MODIS

1. Introduction

With the trend of global warming and the intensification of anthropogenic activities, outbreaks of harmful algal blooms (HABs) have become increasingly serious in both intensity and frequency (Shumway, 1990, 1995; Anderson et al., 1995. HABs were societally defined as an increase in the concentration of phytoplankton species that had negative impacts on surrounding environment (Smayda, 1997). The universally recognized definition mainly contains two aspects, one is the toxic species that release toxin to aquatic creatures or humans, and the other is non-toxic species impact on the environment indirectly through high biomass accumulation (Stumpf and Tomlinson, 2005; Wells et al., 2015). Due to the transient and unpredictable nature of HABs, satellite data has been widely used in observing HABs for inland and near-coastal waters (Kahru et al., 1993; Subramaniam et al., 2002; Kahru et al., 2005; Kutser et al., 2006; Kahru et al., 2007; Matthews et al., 2010), such as MEdium Resolution Imaging Spectrometer (MERIS) (Gower et al., 2005; Gower et al., 2008; Matthews et al., 2010; Binding et al., 2013), Sea-viewing Wide Field-of-view Sensor (SeaWiFS) (Shanmugam et al., 2008), Moderate Resolution Imaging Spectrora diometer (MODIS) (Hu, 2009; Siswanto et al., 2013), Geostationary Ocean Color Imager (GOCI) (Hu et al., 2014), Landsat Data Continuity Mission (LDCM) (Irons et al., 2012) (including MSS/TM/ETM$^+$/OLI), HJ-CCD (Oyama et al., 2015; Xing and Hu, 2016), and so forth. The corresponding spatial and spectral resolution information could be found in Appendix I.

Nowadays, more and more researches are devoted to exploring the relationship between HABs and biological or environmental factors such as temperature, precipitation and lake morphometric features of lakes in South China (e.g., Hu et al., 2010; Yang et al., 2013; Jiang et al., 2014; Wu et al., 2014; Shi et al., 2015; Luo et al., 2016; Shi et al., 2017). Most phytoplankton prefer moderate environmental factors (Wang et al., 2008) and the optimum temperature for many phytoplankton is usually 20~26 ℃ (Cloern, 1977; Rhee and Gotham, 1981). Li et al. (2016b) found that moderate high temperatures could accelerate the formation of cyanobacteria blooms in Lake Taihu, which became an inhibiting factor once exceeded above 33 ℃. Some experts (Jacobs et al., 2015; Wells, 2015) also proposed that the outbreaks of HABs may expand both in time (seasonality) and space (geographical distribution) along with global warming. However, there have been no attempts to use satellite data for monitoring the summer HABs in Northeast China, which has a long ice period. Lake

* Corresponding author. Tel.: 86-431-85542364; fax: 86-431-85542298.
E-mail address: songkaishan@iga.ac.cn (K.S. Song).

ISSN: 1726-2135 print/1684-8799 online
 doi:10.3808/jei.201700385

Hulun is the fifth largest lake in China, which lies in Mongolian Plateau and has significantly ecological and economic importance. MODIS and LDCM were used to map spatio-temporal change of HABs in Lake Hulun, because MODIS has daily reflectance dataset and LDCM data has 30 m spatial resolution with long data acquisition history.

The objective of this paper could be summarized as follows. Firstly, an adjusted FAI method was proposed to enhance the difference in value between HABs and other objects information and an automatic method was test to select the threshold. Secondly, the spatial and temporal distributions of HABs of Lake Hulun in summer are investigated. Thirdly, we preliminary explored the mechanisms to elucidate the observed patterns, such as environmental factors, total phosphorrus (TP), total nitrogen (TN) and TN / TP (nitrogen-phosphorus ratio). The study is of great significance for protecting the lacustrine ecosystems, as well as building monitoring and forecasting programs.

2. Materials and Methods

2.1. Study Area

Lake Hulun is the fifth largest freshwater lake in China, and the largest lake in Northeast China. This lake is located at the west of the Great Khingan Mountains and the east northern part of the Mongolian Plateau as shown in Figure 1. In recent decades, this lake has experienced severe declines in its surface area (from 2047 to 1748 km^2) and water level (from 543.8 to 540.9 m) from 1984 to 2012. Until 2016, the lake had a surface area of 2054 km^2 and a mean depth of 5 ~ 6 m. With an approximate 150,000 km^2 catchment area, Lake Hulun has been mainly fed by two major river systems, the Kerulen River and Wuerxun River (Zuansi et al., 2016), and drains off water into Xinkai River. However, the water level has declined in the past two decades, Xinkai River has become an inflow river (Chen et al., 2012). This gradually results in lacustrine eutrophic intensification and could provide excellent conditions for HABs.

The three nearest meteorological stations surround Lake Hulun are the Manchuria, new Barag right banner and new Barag left banner, as shown in Figure 1. Therefore, the meteorological data were obtained with the average of the three above-mentioned stations. This region is in the semiarid continental temperate monsoon zone, where ample synchronous precipitation and high temperature occur in the summer. The annual average precipitation is around 273 mm, which is mostly distributed in June, July, August and September (Figure 2). Lake Hulun has a long icebound period and only five warm

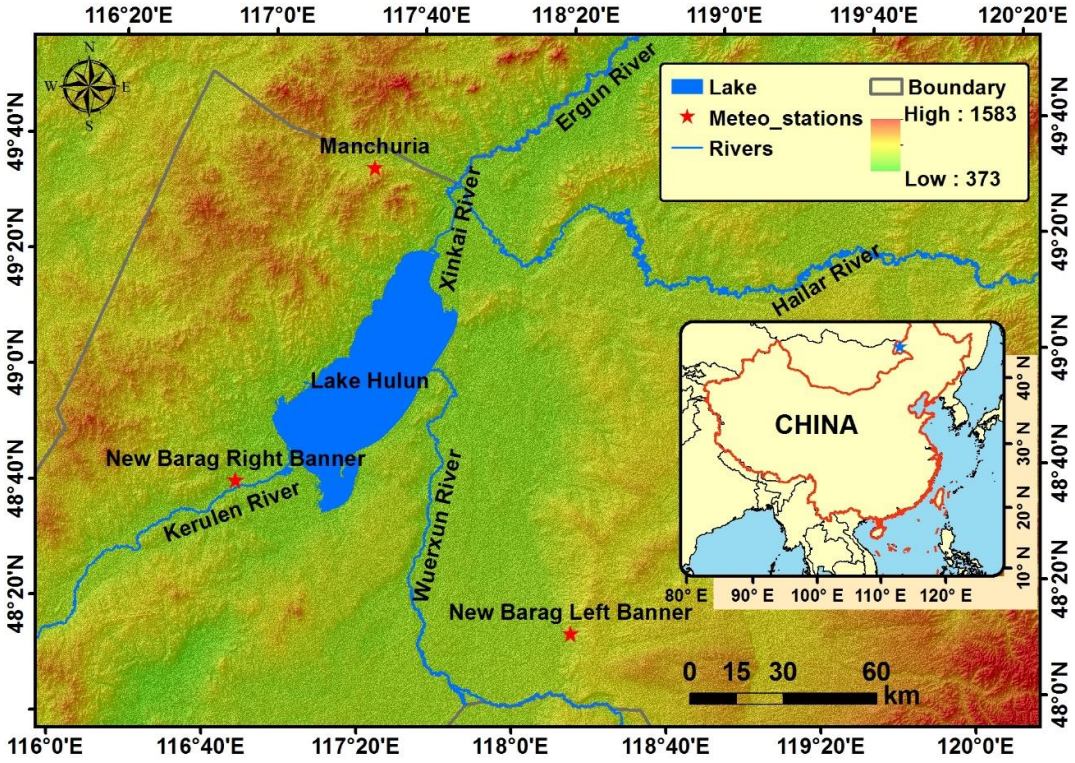

Figure 1. Location and topography distribution of Lake Hulun and its surrounding meteorological stations, China.

Note: Kerulen River and Wuerxun River had been the major inflow rivers of Lake Hulun. Xinkai River was the main outflow river. Since the water level has been declining in the past two decades, Xinkai River has become an inflow river of Lake Hulun in recent years.

months from May to September for each year, where the average temperature is around 0.67 °C.

2.2. Satellite Data and Pre-processing

The satellite data of LDCM images, which had annual coverage from early May to late October each year from 1983 to 2016 (until September 30th in 2016), were acquired from USGS Global visualization viewer web (http://glovis.usgs.gov/) and included MSS, TM, ETM+ and OLI data. The Digital Number (*DN*) of the LDCM images was calibrated to the top-of-atmosphere reflectance ρ_{TOA} with the following equation (1):

$$\rho_{TOA} = \frac{\pi\left(gain \times DN_{\lambda} + offset\right)d^2}{ESUN_{\lambda}\cos\theta_s} \quad (1)$$

where d is earth-sun distance in astronomical unit; θ_s is sun elevation in degree; $ESUN_{\lambda}$ is solar irradiance in unit of W/(m^2 * μm); gain and offset are parameters to convert *DN* to radiance which were obtained from the metadata of the LDCM data.

MOD09GA and MYD09GA are daily surface reflectance products of Terra, and Aqua, respectively. Both of them were downloaded from NASA's Land Processes Distributed Active Archive Center (LP-DAAC). We obtained the MOD09GA products from June 15th to October 30th of every year from 2000 to 2016 (images only covering June 15th to September 30th in 2016). Moreover, hundreds of MYD09GA were also provided as complementary. The MODIS reprojection tool (MRT, Land Processes DAAC, 2008) was used to process MOD09GA and MYD09GA by selecting band 1 ~ 7 and band QC from original HDF file and reprojecting them to Albers projection from original sinusoidal projection.

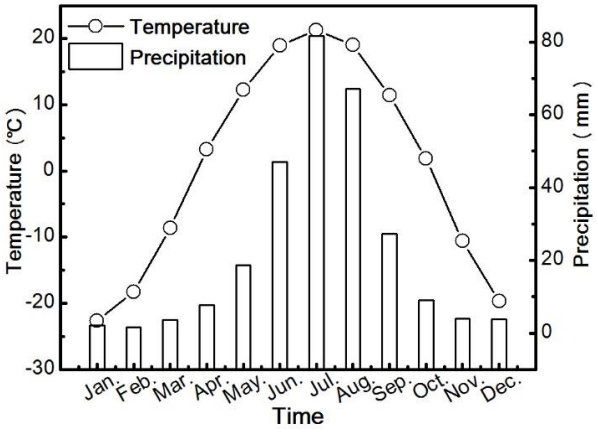

Figure 2. Monthly variation of climatological conditions (Temperature and precipitation) for Lake Hulun.

Note: The closest meteorological stations from Lake Hulun are Manchuria, New Barag Right Banner and New Barag Left Banner (Figure 1). The temperature and precipitation were average of the three stations monthly statistics from 1983 to 2015.

In addition, MODIS products require quality evaluation to guarantee precision of the results. Since severe water level declines in Lake Hulun were revealed during 2000 ~ 2010 (Cai et al., 2016), lacustrine surface area also experienced great fluctuation; therefore, it was necessary to extract water boundary before identifying HABs. Some aquatic macrophytes have similar spectral characteristics around the Near-Infrared (NIR) region (Dekker et al., 2001; Gower et al., 2005), in order to avoid the interference of offshore aquatic macrophytes, we masked one pixel inward from the water boundary. On the one hand, clouds are a pervasive and unavoidable issue in satellite-borne optical imagery (Foga et al., 2017), especially thick cloud entirely hindered the ground reflectance (Lv et al., 2016). Given that restoring the blocked ground reflectance from the original image alone was impossible (Roy et al., 2008), replacement approach (Poggio et al., 2012; Lin et al., 2013; Cheng et al., 2014; Li et al., 2014) and other cloud masking algorithms (Wang and Shi, 2006; Liu and Liu, 2013) were too complicated and ultimately unnecessary for this study, so we regarded the pixel with reflectance greater than 0.2 in green band as cloud region and was counted as invalid pixel after observing abundant images of Lake Hulun, which was reasonable because the water reflectance in green band was far low than 0.2 (Li et al., 2012; Li et al., 2015). On the other hand, valid images were selected by turning to QC band. On user's guide of MODIS surface reflectance, each image has a QC band for recording quality of the corresponding pixels, where the QC value can be further converted to 32-bit binary value by Equation (2). The first two bit figures could describe the integral quality for all bands and the latter bit figures would delineate the detailed quality for per band. In this study, if pixels value in bit locations 15 ~ 18 or 19 ~ 22 were not equal to 0000, green band or SWIR (short wave infrared) would be declared to be bad pixels. Once the total percentage of invalid or bad pixels exceeded 1%, the image would be filtrated to be obsolete and no further efforts would be carried out:

$$\begin{array}{cccccccc} \underset{1\sim 2}{\underline{00}} & \underset{Band\ 1}{\underline{0000}} & \underset{Band\ 2}{\underline{0000}} & \underset{Band\ 3}{\underline{0000}} & \underset{Band\ 4}{\underline{0000}} & \underset{Band\ 5}{\underline{0000}} & & \\ & \underset{3\sim 6}{} & \underset{7\sim 10}{} & \underset{11\sim 14}{} & \underset{15\sim 18}{} & \underset{19\sim 22}{} & & \\ & & & \underset{Band\ 6}{\underline{0000}} & \underset{Band\ 7}{\underline{0000}} & \underset{31}{\underline{00}} & \underset{32}{\underline{00}} & \\ & & & \underset{23\sim 26}{} & \underset{27\sim 30}{} & & & \end{array} \quad (2)$$

2.3. Water Quality Parameters

Water quality parameters were obtained from three field experiments which carried out on September 7th in 2013, September 14th in 2015 and August 11th in 2016. The numbers of sampling points were 7, 28 and 10 in 2013, 2015 and 2016, respectively (Figure 3).

These sampling points covered nearly the whole lake. Water samples, which were about 0.5 ~ 1 m beneath the water surface, were collected using sampling bottles and their

volumes were at least 4 L for each sampling point. At the same time, a portable multi-parameter water quality probe (YSI-6600, US) was used to collect several physical and chemical parameters on site, e.g., temperature, pH, and water depth. Water samples were preserved in a portable refrigerator before taking to a laboratory where other parameters were obtained. The Chlorophyll a (Chl-a) was extracted by using 90% buffered acetone and the concentration was measured using a TD-700 Fluorometer (Turner Designs, Inc., Sunnyvale, CA) following EPA Method 445.0 (EPA, 1997). Concentrations of TN and TP were measured with unfiltered water samples, the details of the operations can be found at Song et al. (2012) and Wen et al. (2016). Also, the TP data of Lake Hulun in 2004 ~ 2014 were obtained from previous paper (Tuan and Yue, 2015).

2.4. Meteorological and Land Cover Data

The data of three meteorological stations (Figure 1) were obtained from Chinese Meteorological Data Sharing Network. The meteorological data covered 34 years from January 1st of 1983 to May 31th of 2016. Mean value of three stations were calculated for all the meteorological elements except for precipitation which only took the closest station new Barag right banner. Surrounding LUCC were obtained from the geographical landscape group in the Northeast Institute of Geography and Agro-ecology, Chinese Academy of Sciences.

Many researchers have found that the first outbreak date and area of HABs were two major parameters (Ma et al., 2010). A simple synchronous variation trend analysis was carried out among the annual HABs areas, first outbreak date, water level, temperature and precipitation.

2.5. Modification of FAI

2.5.1. Introduction of FAI

The FAI (Floating Algae Index), which was proposed by Hu (2009), has been applied mainly to MODIS Rayleigh scattering effects corrected reflectance (Rrc) images. The R_{rc} (Hu et al., 2004; Hu, 2009) can be expressed as:

$$R_{rc} = \pi L_t^* / \left(F_0 \cos\theta_0\right) - R_r \tag{3}$$

where L_t^* is the calibrated sensor radiance with the effects of ozone and other gaseous absorption being removed; F_0 is the extraterrestrial solar irradiance at data acquisition time; θ_0 is the solar zenith angle; and R_t is Rayleigh reflectance estimated with 6S (Vermote et al., 1997; Hu, 2009). Since this process mainly relied on the SeaDAS platform, this method is denoted by SeaDAS way for convenience. The floating algae

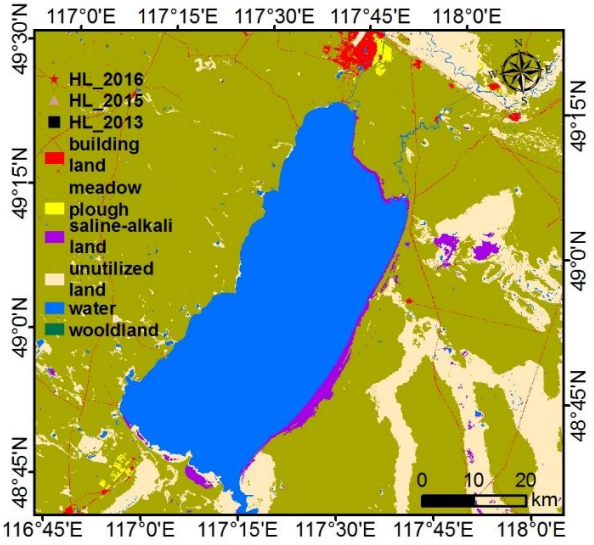

Figure 3. The surrounding land cover type of Lake Hulun and field samples distribution.

Note: HL_2016 represents the points in August 11th of 2016, HL_2015 describes the samples in September 14th in 2015 and HL_2013 expresses the dots in September 7th of 2013.

index was calculated with Equation (4) (Hu, 2009):

$$\begin{aligned} FAI &= R_{rc,\,NIR} - R'_{rc,\,NIR} \\ R'_{rc,\,NIR} &= R_{rc,\,RED} + \left(R_{rc,\,SWIR} - R_{rc,\,RED}\right) \times \\ &\quad \left(\lambda_{NIR} - \lambda_{RED}\right) / \left(\lambda_{SWIR} - \lambda_{RED}\right) \end{aligned} \tag{4}$$

where $R'_{rc,NIR}$ is the simulative reflectance in the NIR band derived from a linear interpolation between the RED and SWIR bands. $R_{rc.X}$ and λ_X represent corresponding reflectance and central wavelength of band X. The central wavelength of the sensors applied in this research were shown in Table 1. Ma et al. (2010) suggested the FAI could also be used to LDCM.

2.5.2. Adjusted FAI

Based on FAI, this paper proposed an adjusted FAI (AFAI) which had two major differences from FAI. The first one was the data source. The FAI used the reflectance data derived from MODIS L0 data, where a series of atmosphere correction was carried out to eliminate the noise in atmospheric molecules such as ozone. In particular, the crucial step for FAI was to calculate Rayleigh scattering value and remove it. However, in this paper, the image sources are MOD-09GA and MYD09GA. According their user's guide, the MOD09 GA/MYD09GA was an estimation of the surface spectral

Table 1. The Center Wavelength of Different Sensors

Sensor Name	MODIS/nm	MSS/nm	TM/nm	ETM+/nm	OLI/nm
Green	555	550	569	560	516.3
Red	645	650	660	662	654.6
NIR	859	757	840	835	864.6
SWIR	1240	916	1676	1648	1609

reflectance after removing not only atmosphere absorption and Rayleigh scattering but also aerosol scattering. In order to make a fair comparison between images processed by the SeaDAS way and directly acquired products, we selected the MODIS L0 and MYD09GA images on July 27th of 2012 and August 12th of 2003 for analysis as HABs were observed on both dates. Atmosphere absorption and Rayleigh scattering affects were removed from MODIS L0 images with SeaDAS. Then the spectra of HABs regions were obtained from the images and shown in figures 4a, 4b, 4d and 4e. Mean spectra of this regions were also calculated. From the ((a) ~ (b)) and ((d) ~ (e)) of Figure 4, the range of the entire image spectra is very similar, and the shapes of waves are almost identical. The (c) and (f) of Figure 4 clearly showed that the peak at 859 nm of MYD09GA which is more evident than the result obtained by SeaDAS way. Based on these results, it is uitable to use the MOD09GA / MYD09GA to extract HABs with FAI and AFAI.

The second difference is the computational formula. The center wavelength ratio played an important role in FAI; however, it was found that although different satellite images had different central wavelengths in green, red, NIR or shortwave infrared band as listed in Table 1, all of the spectra in algal blooms regions shared similar waveforms. According to previous studies, specific features necessary for algal blooms detection included 680 ~ 715 nm (Gitelson, 1992), 708 nm (Gower et al., 2005), and 709 nm (Matthews et al., 2012), yet the LDCM and MODIS bands are relatively wide and cannot capture them. Furthermore, algae floating on the water surface have higher reflectance in the NIR than in other bands, and can be easily distinguished from surrounding waters (Hu et al., 2009). Therefore, it does not matter much where the exact central wavelengths of these bands are as long as the bands are wide. The center wavelength can be ignored and the AFAI can be defined as:

$$AFAI = R_{rc,\,NIR} - R_{rc,\,RED} - \left(R_{rc,\,SWIR} - R_{rc,\,RED}\right) \times 0.5 \qquad (5)$$

Followed the same definition in FAI algorithm, $R_{rc,\,NIR}$, $R_{rc,\,RED}$ and $R_{rc,\,SWIR}$ denote the reflectance of the NIR band, RED band and SWIR band, respectively. The constant coefficient 0.5 was derived according to ($Order_{NIR} - Order_{RED}$) / ($Order_{SWIR} - Order_{RED}$), where *Order* represents the order of ea- ch band in multi-band images (e.g., in MOD09GA/MYD09GA, the expression was $(4-3)/(5-3)$ which is equal to 0.5).

2.5.3. AFAI Threshold Determination

Finding a proper threshold is a crucial step to identify algal blooms in clear water bodies. In general, visual interpretation is feasible in many scenarios (Miller et al., 2006; Hu, 2010; Kurekin et al., 2014; Anderson et al., 2016; Song et al., 2016); however, it consumes too much time and energy investment, and causes extraction results to be varied from one researcher to another (Hu, 2010). Although the following FAI algorithm is much more objective and robust (Hu, 2010), it is arbitrary to initialize a constant value and apply it to all images. If an optimal threshold is determined for each image, the accuracy of extractions could be improved significantly. For this purpose, an automatic threshold selection method was applied to find the most optimal threshold.

After extracting lake (or reservoir) boundary by MNDWI (Xu, 2006) and buffering towards inside one pixel, the HABs threshold selection is carried on AFAI image with the following steps. First, Pixels with AFAI greater than the initial threshold 0 was identified as HABs region. Second, the initial HABs region was dilated until it was about 2 times of the original size to include some initial water region; then histogram curve of AFAI in the expanded region could show two peaks that one mainly contained clear water pixels and the other one for HABs pixels. Third, from the minimal AFAI value on, compute the sum of the left and right standard deviations of the value, the optimal threshold was the value that could get the minimize data of the sum. Then, the threshold could be applied to extract the algal blooms region in corresponding image. In case of systematic error, a data range would be set in advance. After several tests, a valid threshold boundary (0.01 ~ 0.02 for LDCM and 0.05 ~ 0.12 for MOD09GA/MYD09GA) was set. As it is well known (e.g., Jiménez-Muñoz et al., 2010; Mannschatz et al., 2014; Jaelani et al., 2015; Pan et al., 2017), atmospheric correction is necessary for the processing of satellite image and it is still a major challenge to carry out atmospheric correction for inland waters. Therefore we were not able to get absolutely accurate water reflectance until now. Compared to the traditional method with a certain threshold, this method took the differences into consideration the differences among satellite images from different phases, which could find more appropriate thresholds to extract HABs, both keep the precision of extraction in most extent and conformity of various phases.

3. Results and Discussions

3.1. The Reliability Analysis of AFAI

3.1.1. The Advantages and Precautions of AFAI

Compared with FAI algorithm, AFAI algorithm has the following advantages. Firstly, AFAI algorithm makes the reflected peak in NIR more prominent; it compacts the distance among same objects and makes it easier to distinguish HABs and clear water.

Secondly, the overlook of central wavelength could improve the normalization of different sensors and make the computed results unaffected by the central wavelength, which would motivate researchers to extract HABs more efficiently and combine various satellite images.

Thirdly, an unfixed threshold contributes to more precise results. Two different high-quality images of HABs at roughly the same time were chosen. The sensor time of Landsat and Terra were 2000-07-18 02:34:21 and 2000-07-18 02: 35:00 (UTC time), respectively, and there was only a difference of 39

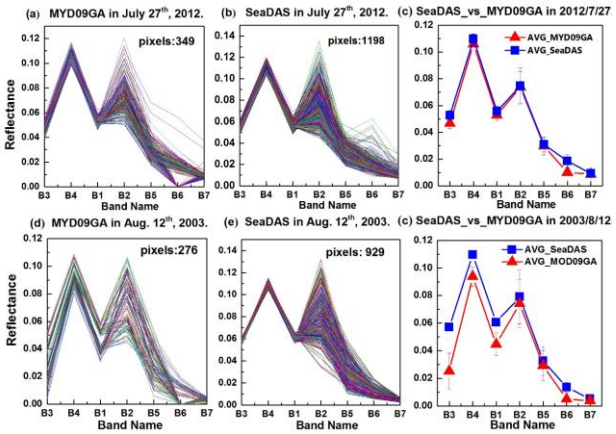

Figure 4. A comparison between the image visual interpretation effects processed by SeaDAS way and directly acquired MODIS products.

seconds. Since the average wind speed was 1.83 m/s on that day, the maximal drifting distance could not exceed 71.37 m, far less than 500 m (MOD09GA spatial resolution). Therefore, it was presumed that the two images had the same HABs. Based on the presumption, algae region and water region were extracted from LDCM. Then the AFAI image and FAI of MODIS images were generated respectively. Finally using algae and water region to export the FAI and AFAI computational value by MODIS (Figure 5c). It could be observed and concluded that all objects could be distinguished more easily via a threshold using the compact AFAI data rather than the FAI data.

However, this algorithm still could not tackle the interference of clouds and vegetation. Therefore, a maximum reflectance of 0.2 in the green band was set to avoid cloud regions, and different phase images were compared to distinguish vegetation. Optical properties of the surface scum produced by some species are similar to those of terrestrial vegetation (Kutser, 2004) and are prone to be masked in the water extraction step, thus later visual interpretation and examination was necessary.

3.1.2. The Regression Analysis between Two Sensors

Monitoring the dynamic variation of HABs at a regular frequency required high spatial and temporal resolution, but a single sensor could hardly meet these two requirements simultaneously. However, the combination of multi-sensors could collect various data from different parts of the electromagnetic spectrum, at different spatial scales, and with different temporal resolutions (Hollands and Dierking, 2016). Therefore, LDCM and MODIS images were used in this paper. In order to inspect and ascertain the error caused by differing resolution and generate the monitoring result in a scientific and reasonable manner, a regression analysis was conducted between the HABs area extracted from MODIS and LDCM images on the same day (Figure 6).

Based on the regression result, there was an obvious linear trend in Figure 6. The R_2 was 0.881 which indicated a strong correlation between the HABs area extracted by MODIS and LDCM. Moreover, the slope was close to 1 which further implied that the consistence of HABs area extracted by LDCM and MODIS images. However, there were two particular points (Point 1 and Point 2) located far away from the regression line. Point 1 represented the results of 12th August,

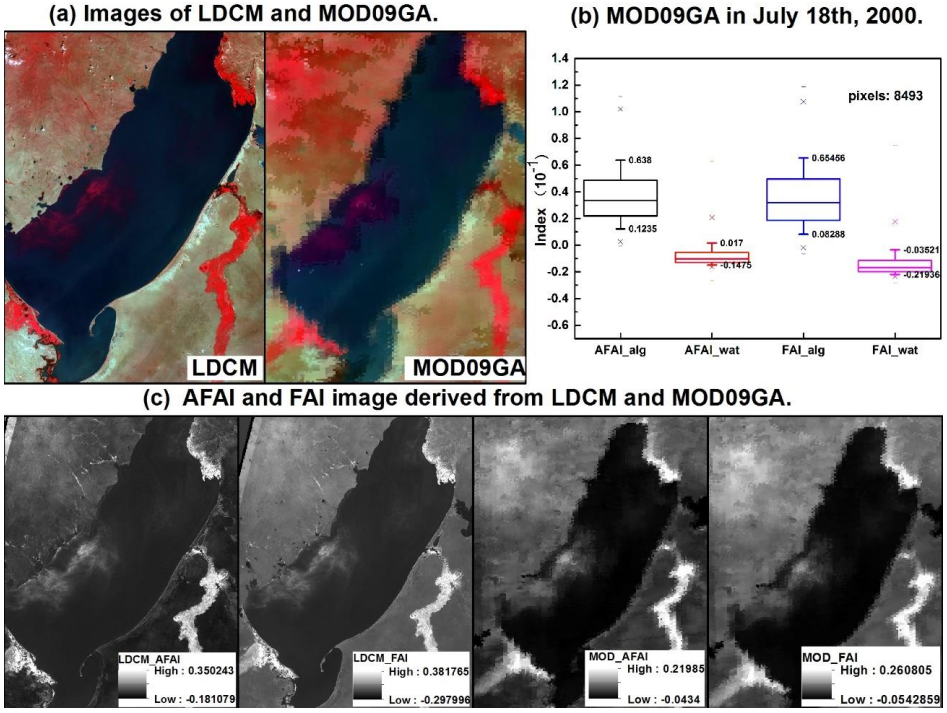

Figure 5. The comparison of AFAI and FAI in algal bloom region and clear water body region.

Table 2. The Monitoring Statistics of HABs via All Useful Images of MOD09GA and MYD09GA During June-October 2000 to 2016

Year	2000		2001		2002		2003		2004		2005		2006		2007		2008	
Time	A	T	A	T	A	T	A	T	A	T	A	T	A	T	A	T	A	T
Jun.	0	0	0	0	0	6	0	7	0	4	0	0	0	0	0	5	0	4
Jul.	4	7	1	10	1	5	2	6	3	13	0	12	0	6	1	13	2	11
Aug.	3	8	0	15	0	10	3	11	4	16	0	22	3	12	1	16	6	15
Sep.	2	17	0	14	2	16	0	15	1	11	0	18	0	27	0	26	0	19
Oct.	0	12	0	24	0	12	0	23	0	21	0	15	0	21	0	22	0	13
T	9	44	1	63	3	49	5	62	8	65	0	67	3	66	2	82	8	62
Year	2009		2010		2011		2012		2013		2014		2015		2016		Total	
Time	A	T	A	T	A	T	A	T	A	T	A	T	A	T	A	T	A	T
Jun.	0	2	1	13	0	6	0	6	0	7	2	7	0	8	0	5	3	80
Jul.	4	15	8	15	8	12	6	8	6	9	10	17	8	16	4	16	68	191
Aug.	5	12	0	10	3	20	1	13	7	13	0	13	2	12	2	14	40	232
Sep.	1	11	0	20	0	17	0	18	0	16	5	23	3	12	4	11	18	291
Oct.	0	15	0	18	0	24	0	20	0	15	0	20	0	19	0	0	0	294

* The letter A represents the number of found algal blooms images, the letter T represents the total number of images.

2009: the data source of LDCMs and MODIS was respectively TM (in antemeridiem) and MYD09GA (in the afternoon). On that day, the average wind speed was 3.1 m/s and the maximum wind speed was recorded as 9.5 m/s; the strong wind affected the distribution and modalities of HABs significantly in an unavoidable manner. Thus, there was a notable variation of the two detection results. Similarly, Point 2 could also be explained by the same argument. In conclusion, the comparison and analysis above demonstrated the MODIS images could be an alternative data source for HABs detection of Lake Hulun with high temporal resolutions.

3.2. The Frequency Variation of HABs

In order to identify the spatiotemporal change of HABs in Lake Hulun, a total of 380 scenes of available LDCM images from May to October, 1983-2016 were downloaded from USGS website (Appendix II). A total of 64 images were detected with HABs. Figure 7 showed the percentage ratio and the specific surface area of the lake change trend and the temporal pattern of HABs. Generally, HABs outbroke from June to September; June, July, August, and September accounted for approximately 3.2, 48.4, 32.8 and 15.6%, respectively. In addition, serious HABs mostly occurred in July and August. Since the count of images available from 1983 ~ 1999 and 2000 ~ 2016 were not in an order of magnitude, the analysis of the inter-annual bloom frequency variation had to be divided into two parts. In the first 17 years (1983 ~ 1999, Figure 7a), no obvious trend could be found and there were total 10 years found HABs. The change of percentage was mostly consistent with the dynamic of area, which implied that during this period, the water level were keeping relatively stable. In the second 17 years (2000 ~ 2016, Figure 7b), a gradually higher frequency and the severity of HABs could be detected especially after 2009 and total 16 years were observed HABs. Moreover, the coherence of area and percentage change became much weaker. Which indicated that in this phase, the deterioration of the lake quality was intensified and lake surface area also fluctuated frequently and significantly.

Additionally, 3208 scenes of MODIS products, contained 2256 scenes of MOD09GA images and 952 scenes of MYD09GA, were acquired from Terra and Aqua in June ~ October each year of 2000 ~ 2016. Additionally, 1088 scenes were of high quality (Table 2). From Table 2, the total number of images where HABs were found was 129. Although it could only account for 11.86 % of the total 1088 images, there were still approximately 7.5 outbreaks on average each year from 2000 to 2016. The frequency of HABs was considered extremely high for the famous tourist scenic spot. In terms of monthly difference, the two highest frequencies of blooms were in July and August, which were around 52.71 and 31.01 % of the total number, respecttively. Moreover, the third and fourth highest frequency of blooms were in September and

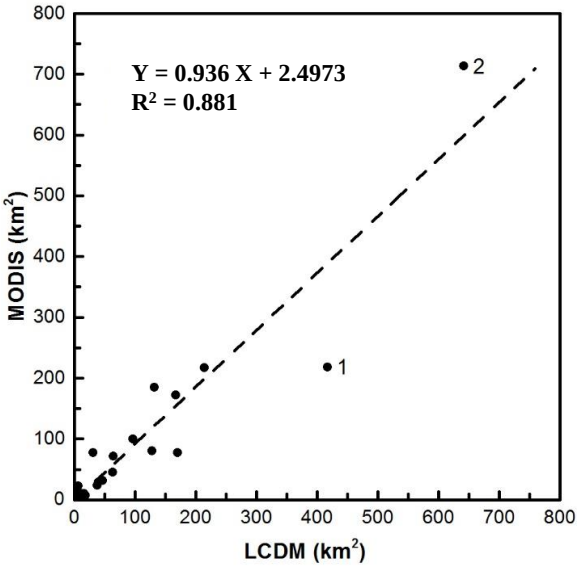

Figure 6. The regression analysis of HABs area at the same day of MODIS and LDCM images.

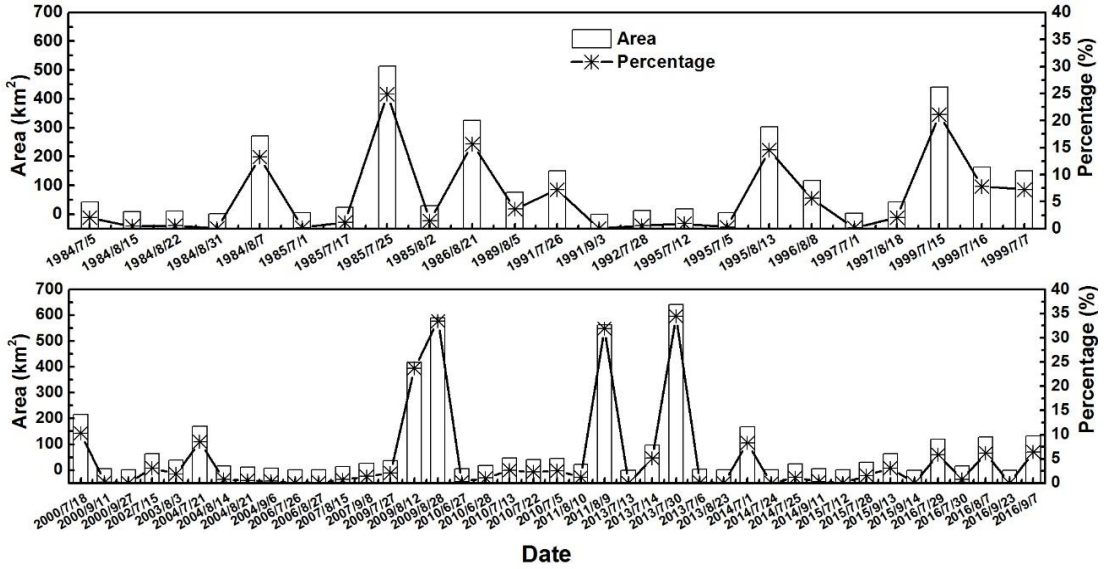

Figure 7. All the detected area and percentage variation of HABs inferred from the LDCMs images during May ~ October in 1983 ~ 2016.

June, which further proved that there would be more favorable conditions for HABs from June to September each year. In contrast, there were no HABs found in October.

In addition, some anomalous MODIS images were found on some dates because nearly all the pixels of the lake had spectra similar to HABs. This strange phenomenon may be caused by the mixture of dead algae and some suspicious matters, which could not be distinguished by the limited spectral and spatial resolution of the MODIS sensor. Severe noise may also exist in these kind of images and they were abandoned in this research to avoid confusion.

As for inter-annual variation, the year 2009 was a significant watershed. Before 2009, all the outbreak numbers of HABs were less than 9 and the average outbreak numbers were only 4.33. Nevertheless, outbreak frequency of HABs in the years after 2009 increased dramatically and the average number was up to 10, with the exception of 7 times in 2012. The more and more frequent outbreak of HABs demonstrated that the degeneration of water quality in the latest 9 years.

3.3. Spatiotemporal Change of HABs

Recent research showed that wind speed could affect the detection area of HABs. In other words, different wind speeds may lead to different results for detecting the same HABs (Kononen et al., 1996; Sellner, 1997; Wynne et al., 2010), because the gas vacuoles of part algal species (especially cyanobacteria) could adjust the body buoyancy (Walsby et al., 1997; Kutser, 2004). Thus, the biggest area of HABs were regarded as the indicator each year. From 1983 to 2016, a total of 26 years of HABs were detected and the biggest HABs area retrieved from LDCM and MODIS products were selected to map the spatiotemporal change of inter-annual HABs distribution in Lake Hulun (Figure 8).

There are many ways to characterize the outbreak intensity of HABs, e.g., area, AFAI data. In terms of the variation of the surface area, the extremely serious HABs events happened in 1985, 1999, 2000, 2009, 2011 and 2013, and most of them were concentrated after 1999. According to the AFAI data difference (the color from red to light green on the map), most significant outbreaks of HABs mainly happened in 1985, 1999, 2000, 2010, 2013, 2014 and 2015, which were also mostly distributed in the period after 1999.

In terms of the inter-annual continuity of HABs, HABs could be detected subsequently in the years of 2008 to 2016 and 1999 to 2004. However, the phenomenon of HABs distributed sporadically in the other study period. Also, it could be observed that both area and severity of HABs after 2008 were more serious than those before 2004. Above all spatial variation analyses of HABs were only based on the area and inter-annual continuity, lacking the specific spatial distribution state of HABs in Lake Hulun in the last few decades. In order to visualize the spatial change statics, an algorithm was proposed in this paper as shown in Equation (6):

$$f(x)=\begin{cases}1, x\in HAB_s\\ 0, x\notin HAB_s\end{cases}$$
$$g(x)=\sum_{i=1}^{n} f(x), i=1,2,\ldots,n \quad (6)$$

where $f(x)$ is the elementary statistic computed from each image, and $g(x)$ is the final data mapped in Figure 9. The total number of images participating in the operation is denoted by n.

After above computation, two images could be acquired and showed in Figure 9. Both images were classified into 5

degrades. A total 53 scenes of LDCM images were analyzed in Figure 9a and the highest frequency of HABs was 13 times. Meanwhile, 106 scenes of MODIS products were computed in Figure 9b and the highest frequency was 18 times. It could be observed that the spatial variaton were consistent between the LDCM and MODIS. HABs almost covered the entire lake surface and the outbreak frequencies were decreasing gradually from the southwest and northwest to the middle region. In particular, the frequency was pretty high at the lake edge, which was possibly caused by the cover type of adjacent land and the water velocity in the neighboring area. Moreover, the frequency in the southwest region was extremly high because the region was close to the estuary of the Kerulun river (Figure 1). The Kerulun River was a major inflowing river of Lake Hulun and thus the water quality of the lake was closely dependent on the river. A number of studies have shown that

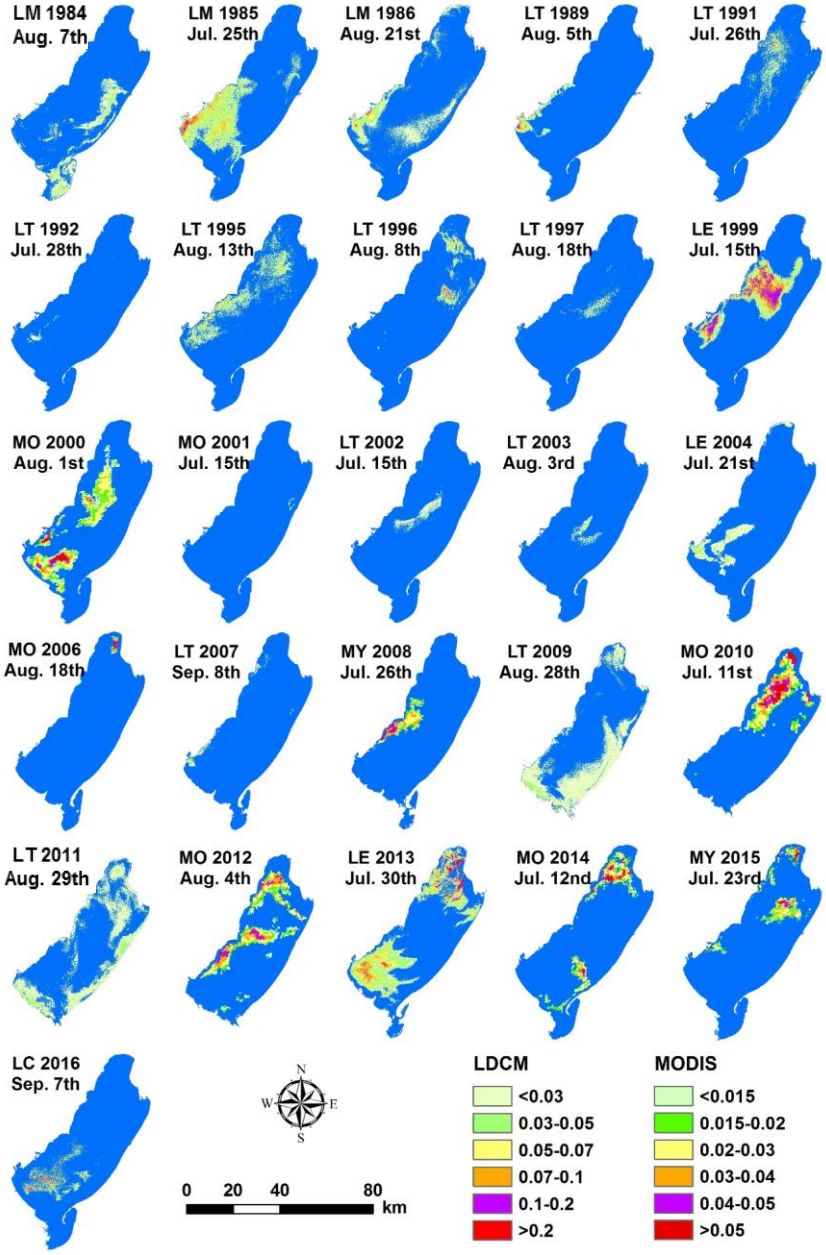

Figure 8. Spatial and temporal change of inter-annual HABs distribution in Lake Hulun. Note: LM, LT, LE and LC represent the image obtained from MSS, TM, ETM+ and OLI of LDCM respectively. In addition, MO and MY simplified the product of MOD09GA of Terra and MYD09GA of Aqua. Since there are a great difference between the AFAI image computed from LDCM and MODIS products, two sets of distinguished legends are needed and divided into 6 degrades according to AFAI data. It indicated the severity of HABs in some extent. The legend titled LDCM was degraded in LM, LT, LE and LC, and the titled MODIS was degraded into MO and MY.

the Kerulun River had been sufferring from various pollutions in recent decades, e.g., grazing in both river banks, cooked leather factories, nitrate factories and so forth (Li et al., 1993; Liang et al., 2016), which concentrated the TP and TN of the estuary drastically (Li et al., 2016a). As a result, the highest frequency of HABs was distributed in this region. The sub-high-frequency area of HABs was close to the estuary of the XinKai River. When the Hailar River had a higher water-level than the Xinkai River, it would then become a major industrial waste water discharged by different factories such as paper mills, leather factories, and woolen mills along the Hailar River (Figure 1). However, because the Hailar River was distant (resulting in a certain degree of purification) and the the Ergun River was in a state of stagnation for more than half a year (Li et al., 1993), the pollution resulted from these rivers in northwest water area was less than southwest. In conclusion, the analyses above demonstrated that the water quality of the surrounding river esuary could influence the spatial distribution of HABs. Therefore, it is critical to improve water conditions of inflowing rivers in order to control the HABs in Lake Hulun.

3.4. Preliminary Analysis on the Driving Factors

A number of researches have been focusing on HABs recently; however, there is still no tenable hypothesis of how climate pressures (Wells et al., 2015) or other factors mechanistically affect HABs until now. This could be explained by the following two reasons: the mechanism is pretty complex and the outbreaks of HABs are generally influenced by multiple factors, e.g., temperature (Bissenger et al., 2008; Eppley, 1972), stratification (Figueras et al., 2006; Smayda and Trainer, 2010), light (Anderson et al., 1987; Bravo and Anderson, 1994; Anderson et al., 2005;), precipitation-induced nutrient inputs, grazing (Wells et al., 2015) and exogenous inputs of rivers. Therefore, this paper emphatically analyzed the effects of temperature, precipitation and water level on the first outbreak date and area, and made preliminary explanations about how those factors affected the HABs of Lake Hulun.

3.4.1. Meteorological Factors

From Figure 10, the first outbreak date of each year fluctuated significantly but overall became earlier (Figure 10b), which implied the outbreak date was earlier and earlier. In some years with relatively high temperatures (Figure 10d), e.g., 2000, 2007, 2009, 2011 and 2014, the outbreak of HABs happened fairly early. In several low-temperature years, e.g., 1987, 1988, 1990 and 2005, there were no HABs phenomenon found. However, not all of the periods followed the same principle: there were some years with relative high temperatures yet accompanied with posterior outbreak dates. This is still reasonable as the mechanisms affectting HABs included more factors besides the temperature.

In recent decades, the water level of the Lake Hulun has been suffering a severe fluctuation (Figure 10c), and the overall period could be classified to three stages. The first stage was before 1986 when the water level elevated dramatically. In this stage, the first outbreak date was firstly slight ahead of time and then largely delay in time. The slight ahead of time might be caused by a large amount of spores lurking under the water from the previous year until the winter. However, before 1986, the water level kept increasing constantly, which could effectively reduce the various concentrations of water quality in order to avoid HABs and delay the first outbreak date. The second stage was relatively stable from 1986 to 1999. During

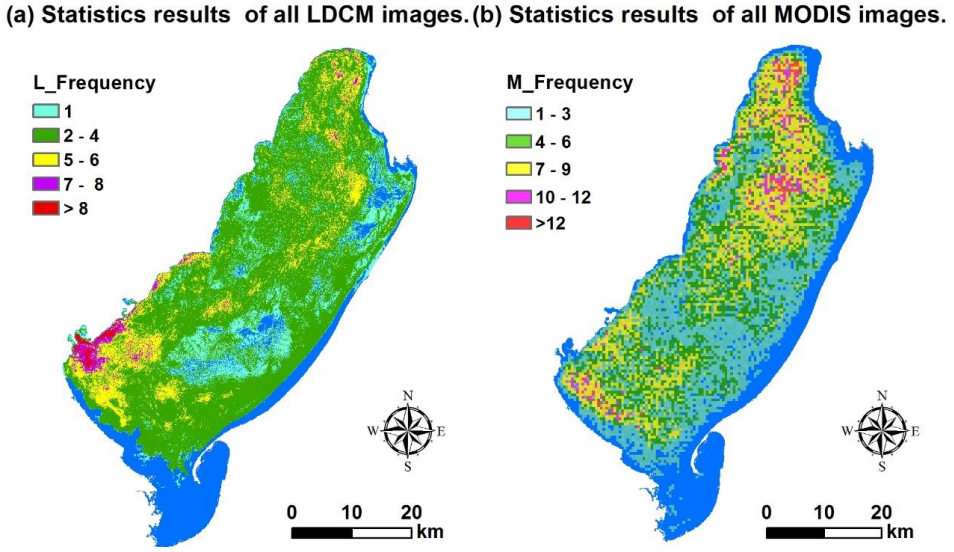

Figure 9. The frequency of HABs spatial distribution in the lake Hulun. (a) the statistics results of all HABs images obtained from LDCMs images in 1983 ~ 2016; (b) the statistic results of all HABs scenes obtained from MODIS products in 2000 ~ 2016, which does not include the images has the same date with LDCMs images to avoid the repeated statistics.

this stage, the frequency of HABs was very low and the overall outbreak number was relatively small. The third stage was the significant decreesing period from 1999 to 2016, which consisted of continuous outbreaks with the exception of 2005. Although the date fluctuated, the overall trend was relatively early, which was also consistent with the negative correlation between the water-level and HABs. Therefore, it is highly possible that low water level cause HABs.

Along with global warming intensification, the temperature of Lake Hulun appeared to rise with some fluctuations, companied by the increase in the frequency and severity of HABs (Figure 10). To some extent, the temperature was positively correlated to the frequency and severity of HABs. Especially in 1985, 1999, 2000, 2009 and 2011, when all the corresponding temperatures were higher than 12 °C. In the relative cold years of 1987, 1990 and 2006, there were only small areas of HABs (Figure 10a) and no blooms could even be detected. This phenomenon further proved the positive correlation between the temperature and HABs. However, some obviously adverse trend between temperature and HABs area could also be observed in 1984, 1995 and 2013 (Figure 10e). During those periods, a reasonable explanation combined with precipitation and temperature could be given as follows: although the temperatures of those years were relatively low, the rainfall was abundant. Note that there was a large area of grassland in the previous introduction about the surrounding land covers of Lake Hulun in Figure 3. The surface runoff caused by precipitation carried massive faeces of livestocks into Lake Hulun and therefore provided favorable bloom conditions. It was very dramatic and hardly feasible to analyze the relationship between precipitation and HABs only, because the precipitation had two different impacts, which was resulted from the river named Xinkai River (Figure 1), that became the inflowing river when the

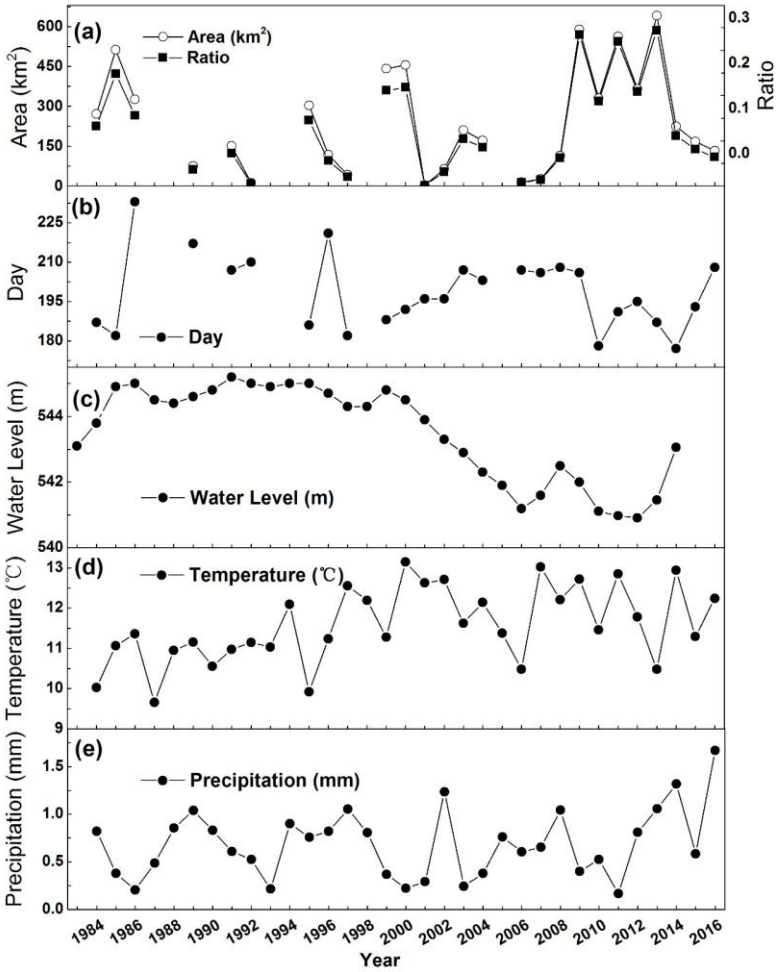

Figure 10. The temporal variation of HABs indexes and multiple natural factors in 1983-2014. (a) Areal coverage of the HABs in Lake Hulun and the proportion of HABs in the total surface water, where the data were extracted from the time series Figure 8; (b) the first outbreak date change trend of HABs from 1983 to 2016; (c) water-level dynamics change of Lake Hulun in 1983-2014; (d) and (e) the meteorological data (temperature and precipitation) change trend from 1984 to 2015 respectively.

water-level was fairly low and the outflowing river while water level was relatively high. The interactive roles of Xinkai River caused different dominant effects of precipitation directly on Lake Hulun. In the same condition of abundant precipitation and the Xinkai River playing an inflowing role on Lake Hulun systems, more nutrients could be transported into the lake. Therefore, there would be a positive correlation relationships between HABs and precipitation. On the other hand, once the water level was high enough and the Xinkai River became an outflowing river to Lake Hulun system, lake water were able to exchange frequently and the concentration of water quality parameters got diluted along with the increase of precipitation.

3.4.2. The Impact of Nutrients

The deterioration of Lake Hulun was resulted from multiple factors. Apart from upstream industrial pollution carried by rivers and flushing of contaminated peripheral land via overland water, the anthropogenic activities in ice age also brought pretty much pollution to Lake Hulun. Located in high latitudes, Lake Hulun had a significantly long ice age, where a mass of contaminants like horse manure were preserved under the ice due to the use of horses as labor by fishing workers. These contaminants were resolved into the water body when the lake thawed (Li et al., 1993). As a scenic tourist attraction, the management mechanisms and infrastructures were imperfect, which resulted in plenty of tourist trash being carried into the lake and deteriorating the water quality (Tuan and Yue, 2014). Those contaminants contained a mass of nitrogen and phosphorus elements, which provided an appropriate chemical environment for HABs.

To explore the impact of the chemical parameters on spatial-temporal variation of HABs, all TP, TN and TN/TP distribution sampled in 2013, 2015 and 2016 were mapped in this paper (Figure 11a). Then the change curve of TP in Lake Hulun was plotted from 2004 to 2016 (Figure 11b). However, since Lake Hulun had a stronger flowing ability from 2013, there was no particular spatial difference of TP, TN and TN/TP. Although a huge fluctuation could be found in the change curve, the TP value in those years was still relatively high. In addition, the average TN measured in 2013, 2015, 2016 was 1.91, 8.5, 1.91 mg/L respectively. Those values were all far above the internationally recognized TP level of 0.02 mg/L and TN of 0.2 mg/L, which could cause eutrophication (Guo et al., 2005). The results implied that the concentration of TN and TP was sufficient enough to provide a favorable environment for HABs outbreak in Lake Hulun and it was no longer a decisive factor affecting the blooming scope and perniciousness.

4. Conclusions

In general, this paper has achieved the following goals. Firstly, the AFAI approach with automatic threshold determination was proposed to extract the HABs shape and area. Secondly, the spatiotemporal distribution of HABs in Lake Hulun was systematically analyzed with LDCM and MODIS images. In particular, the precedent of HABs in northeast Chinese lakes was initiated. Furthermore, multiple factors including meteorological elements (temperature, precipitation and water-level) and chemical parameters (such as TP, TN and TN/TP) were considered for analyzing the comprehensive impacts on the frequency and severity of HABs.

However, there is still a huge potential for further research. The observation of HABs by many satellites is limited because of spatial resolution, even at a smaller spatial scale

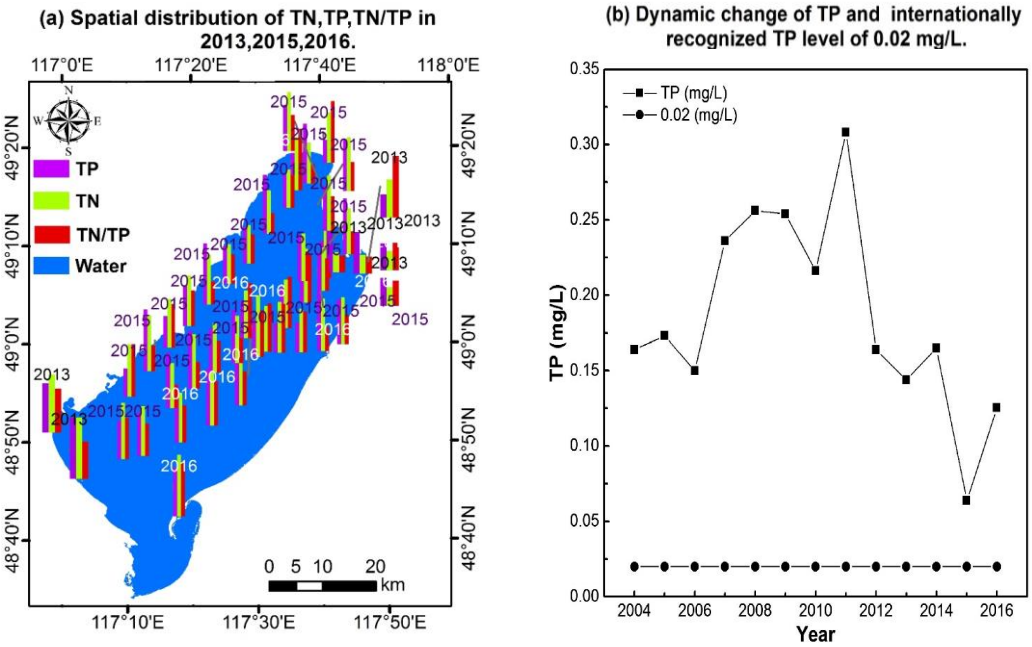

Figure 11. The spatial-temporal variation of some chemical parameters in the surface lake of the Lake Hulun.

than 30 m (Kuster, 2004). Although the AFAI could be desirably used to monitor the HABs of Lake Hulun, it remains unclear whether the method could be similarly used on other lakes or not. Apart from Lake Hulun, there are many lakes in northeast China which have been observed with HABs in recent decades. The spatiotemporal changes in these lakes have not yet been systematically investigated. Since the detecting images are only multispectral but not hyperspectral, specific species of algae can't be distinguished. Therefore, the distribution merely describes all kinds of HABs change.

Acknowledgements. This work is jointly supported by the National Key Research and Development Project (No. 2016YFB0501502), the National High Resolution Earth Observation Systems Projects (41-Y20A31-9003-15/17), and National Natural Science Foundation of China (No. 41471290, No. 41501387). The authors also would like to thank all the staff and master students for their efforts in field data collection and laboratory analysis. Furthermore, special thanks to the research group led by Mr. Wang who provided the land cover data of Northeast Institute of Geographic and Agro-ecology, Chinese Academy of Sciences. Finally, we would like to thank Ge Liu for his help in processing part data via SeaDAS.

References

Anderson, D. M., Taylor, C. D., and Armbrust, E. (1987). The effects of darkness and anaerobiosis on dinoflagellate cyst germination. *Limnol. Oceanogr.*, 32(2), 340-351, DOI: 10.4319/lo.1987.32.2.0340.

Anderson D.M., Stock C.A., Keafer B.A., Nelson A.B., Thompson B., McGillicuddy Jr. D.J., Keller M., Matrai P.A.,and Martin J. (2005). Alexandrium fundyense cyst dynamics in the Gulf of Maine. *Deep Sea Res. (II Top. Stud. Oceanogr.)*, 52(19), 2522-2542. DOI: 10.1016/j.dsr2. 2005.06.014.

Anderson C.R., Kudela R.M., Kahru M., Chao Y., Rosenfeld L.K., Bahr F.L., Anderson D.M., and Norris T.A. (2016). Initial skill assessment of the California Harmful Algae Risk Mapping (C-HARM) system. *Harmful Algae*, 59, 1-18. DOI: 10.1016/j.hal.201 6.08.006.

Binding, C.E., Greenberg, T.A., and Bukata, R.P. (2013). The MERIS maximum chlorophyll index; its merits and limitations for inland water algal bloom monitoring. *J. Great Lakes Res.*, 39(100107), 18. DOI: 10.1016/j.jglr. 2013.04.005.

Bissinger, J. E., Montagnes, D. J., Sharples, J., and Atkinson, D. (2008). Predicting marine phytoplankton maximum growth rates from temperature: Improving on the Eppley curve using quantile regression. *Limnol. Oceanogr.*, 53(2), 487. DOI: 10.4319/lo.2008. 53.2.0487.

Bravo, I. and Anderson, D. M. (1994). The effects of temperature, growth medium and darkness on excystment and growth of the toxic dinoflagellate Gymnodinium catenatum from northwest Spain. *J. Plankton Res.*, 16(5), 513-525. DOI: 10.1093/plankt/16.5. 513

Cai, Z., Jin, T., Li, C., Ofterdinger, U., Zhang, S., Ding, A., and Li, J. (2016). Is China's fifth-largest inland lake to dry-up? Incorporated hydrological and satellite-based methods for forecasting Hulun lake water levels. *Adv. Water Resour.*, 94, 185-199. DOI: 10.1016/j.advwatres.2016.05.010.

Cheng, Q., Shen, H., Zhang, L., Yuan, Q., and Zeng, C. (2014). Cloud removal for remotely sensed images by similar pixel replacement guided with a spatio-temporal MRF model. *ISPRS J. Photogramm. Remote Sens.*, 92, 54-68. DOI: 10.1016/j.isprsjprs. 2014.02.015.

Cloern, J. E. (1977). Effects of light intensity and tempweature on Cryptomonas Ovata (Cryptophyceae) growth and nutrient uptake rates1. *J. Phycol.*, 13(4), 389-395. DOI: 10.1111/j.1529-8817.1977.tb02947. x.

Dekker, A. G., T. J. Malthus, and L. M. Goddijn. (1992). Monitoring cyanobacteria in eutrophic waters using airborne imaging spectroscopy and multispectral remote sensing systems. *Proceedings of Sixth Australasian Remote Sensing Conference*, 1, 204-214.

Eppley, R.W. (1972). Temperature and phytoplankton growth in the sea. *Fish. Bull*, 70(4), 1063-1085.

Gitelson, A. (1992). The peak near 700 nm on radiance spectra of algae and water: relationships of its magnitude and position with chlorophyll concentration. *Int. J. Remote Sens.*, 13(17), 3367-3373. DOI: 10.1080/01431169208904125.

Guo, M., Wang, Z, Peng, C. (2005). The abundance and strucure comparison of purple nonsulfer bacteria between Yangzonghai Lake and Diancchi Lake. *Acta Ecologica Sinica*, 25(6): 1337-1340 (in Chines with English abstract).

Gower, J., King, S., Borstad, G., and Brown, L. (2005). Detection of intense plankton blooms using the 709 nm band of the MERIS imaging spectrometer. *Int. J. Remote Sens.*, 26(9), 2005-2012. DOI: 10.1080/01431160500075857.

Gower, J., King, S., and Goncalves, P. (2008). Global monitoring of plankton blooms using MERIS MCI. *Int. J. Remote Sens.*, 29(21), 6209-6216. DOI: 10.1080/01431160802178110.

Hollands, T. and Dierking, W. (2016). Dynamics of the Terra Nova Bay Polynya: The potential of multi-sensor satellite observations. *Remote Sens. Environ.*, 187, 30-48. DOI: 10.1016/j.rse.2016.10.003.

Hu, C. (2009). A novel ocean color index to detect floating algae in the global oceans. *Remote Sens. Environ.*, 113(10), 2118-2129. DOI: 10.1016/j.rse.2009.05.012.

Hu C., Lee Z., Ma R., Yu K., Li D., and Shang S. (2010). Moderate resolution imaging spectroradiometer (MODIS) observations of cyanobacteria blooms in Taihu Lake, China. *J. Geophys. Res. (C Oceans)*, 115(C4). DOI: 10.1029/ 2009JC005511.

Foga S.,Scaramuzza P., Guo S., Zhu Z., Dilley R., Beckmann T., Schmidt G.L., Dwyer J.L., Hughes M.J., and Laue B. (2017). Cloud detection algorithm comparison and validation for operational Landsat data products. *Remote Sens. Environ.*, 194, 379-390. DOI: 10.1016/j.rse.2017.03.026.

Figueiras, F. G., G. C. Pitcher, and M. Estrada. (2006). Harmful algal bloom dynamics in relation to physical processes. Ecology of harmful algae. *Springer Berlin Heidelberg*, 2006. 127-138. DOI: 10.1007/978-3-540-32210-8_10

Irons, J. R., Dwyer, J. L., and Barsi, J. A. (2012). The next Landsat satellite: The Landsat data continuity mission. *Remote Sens. Environ.*, 122, 11-21. DOI: 10.1016/j.rse.2011.08.026.

Jacobs J., Moore S.K., Kunkel K.E., and Sun L. (2015). A framework for examining climate-driven changes to the seasonality and geographical range of coastal pathogens and harmful algae. *Clim. Risk Manage.*, 8: 16-27. DOI: 10.1016/j.crm.2015. 03.002.

Jaelani L.M., Matsushita B., Yang W., and Fukushima T.. (2015). An improved atmospheric correction algorithm for applying MERIS data to very turbid inland waters. *Int. J. Appl. Earth Obs. Geoinf.* 39: 128-141. DOI: 10.1016/j.jag.2015.03.004.

Jiang Y.J., He W., Liu W.X., Qin N., Ouyang H.N., Wang Q.M., Kong X.Z, He Q.S., Yang C., Yang B.,and Xu F.L. (2014). The seasonal and spatial variations of phytoplankton community and their correlation with environmental factors in a large eutrophic Chinese lake (Lake Chaohu). *Ecol. Indicators*, 40: 58-67. DOI: 10.1016/ j.ecolind.2014.01.006.

Jiménez-Mu-oz J.C., Sobrino J.A., Mattar C., French B. (2010). Atmospheric correction of optical imagery from MODIS and Reanalysis atmospheric products. *Remote Sens. Environ.*, 114(10),

2195-2210. DOI: 10.1016/j.rse.2010.04. 022.

Kahru, M., Leppanen, J. M., and Rud, O. (1993). Cyanobacterial blooms cause heating of the sea surface. *Mar. Ecol. Prog. Ser.*, 1-7. DOI: 10.3354/meps101001.

Kahru, Mati, B. Greg Mitchell, and Anibal Diaz. (2005). Using MODIS medium-resolution bands to monitor harmful algal blooms. *Proc. SPIE*, 5885, 162-167.DOI: 10.1117/12. 615625.

Kahru, M., Savchuk, O. P., and Elmgren, R. (2007). Satellite measurements of cyanobacterial bloom frequency in the Baltic Sea: inter-annual and spatial variability. *Mar. Ecol. Prog. Ser.*, 343, 15-23. DOI: 10.3354/meps06943.

Kononen, K., Kuparinen, J., Mäkelä, K., Laanements, J., Pavelson, J., & Nommann, S. (1996). Initiation of cyanobacterial blooms in a frontal region at the entrance to the Gulf of Finland, Baltic Sea. *Limnol. Oceanogr.*, 41(1), 98-112. DOI: 10.4319/lo.1996.41.1.0098.

Kurekin A A, Miller P I, and Van der Woerd H J. (2014). Satellite discrimination of Karenia mikimotoi and Phaeocystis harmful algal blooms in European coastal waters: Merged classification of ocean colour data. *Harmful Algae*, 31: 163-176. DOI: 10.1016/j.hal.2013.11.003.

Kutser T.(2004). Quantitative detection of chlorophyll in cyanobacterial blooms by satellite remote sensing. *Limnol. Oceanogr.*, 49(6), 2179-2189. DOI: 10.4319/lo.2004.49. 6.2179.

Kutser, T., Metsamaa, L., Strömbeck, N., and Vahtmäe, E. (2006). Monitoring cyanobacterial blooms by satellite remote sensing. Estuarine. *Coast. Shelf Sci.*. 67(1), 303-312. DOI: 10.1016/j.ecss.2005.11.024.

Liang, L. E., Li, C. Y., Shi, X. H., Zhao, S. N., Tian. Y., and Zhang, L. J. (2016). The eutrophication trend and analysis of Lake Hulun in Inner Mongolia from 2006 to 2015 (Chinese), *J. Lake Sci.*, 28(6): 1265-1273.

Li, B.L., Wang, Y.T., and Zhang, L.Z. (1993). Evaluating water contamination and nutrition level of Lake Dalai with phytoplankton (Chinese). *Acta Hydrobiologica Sinica*, 17(1): 27-34.

Li, L., Li, L., Shi, K., Li, Z., & Song, K. (2012). A semi-analytical algorithm for remote estimation of phycocyanin in inland waters. *Sci. Total Environ.*, 435, 141-150. DOI: 10.1016/j.scitotenv.2012.07.023.

Li, L., Li, L., and Song, K. (2015). Remote sensing of freshwater cyanobacteria: An extended IOP Inversion Model of Inland Waters (IIMIW) for partitioning absorption coefficient and estimating phycocyanin. *Remote Sens. Environ.*, 157, 9-23. DOI: 10.1016/j.rse.2014.06.009.

Li, W. P., Chen, A. H., Yu, H. L., Yang, W. H., Yin, Z. Y., Yang, P. F., and Jiao, L. Y. (2016a). Contaminant flux of Lake Hulun major inflow river Kerulen River from 2010 to 2014 (Chinese). *J. Lake Sci.*, 28(2):281-286. DOI: 10.18307/2016. 0206.

Li, X., Shen, H., Zhang, L., Zhang, H., Yuan, Q., and Yang, G. (2014). Recovering quantitative remote sensing products contaminated by thick clouds and shadows using multitemporal dictionary learning. *IEEE Trans. Geosci. Remote Sens.*, 52(11), 7086-7098. DOI: 10.1109/TGRS. 2014.2307354.

Lin, C. H., Tsai, P. H., Lai, K. H., and Chen, J. Y. (2013). Cloud removal from multitemporal satellite images using information cloning. *IEEE Trans. Geosci. Remote Sens.*, 51(1), 232-241. DOI: 10.1109/TGRS.2012.2197682.

Luo, J., Li, X., Ma, R., Li, F., Duan, H., Hu, W., and Huang, W. (2016). Applying remote sensing techniques to monitoring seasonal and interannual changes of aquatic vegetation in Taihu Lake, China. *Ecol. Indicators*, 60, 503-513. DOI: 10.1016/j.ecolind.2015.07.029.

Lv, H., Wang, Y., and Shen, Y. (2016). An empirical and radiative transfer model based algorithm to remove thin clouds in visible bands. *Remote Sens. Environ.*, 179, 183-195. DOI: 10.1016/j.rse.2016.03.034.

Ma, R. H., Duan, H. T., Tang, J. W., and Chen, Z. B. (2010). Remote sensing of water environment in lakes. Science Press, Tuan, L., Yue, C. Y. (2015). Research on the water quality and prevention measures of the Lake Hulun from 2004 to 2014 (Chinese). *Environ. Sci. Manag.*, 40(5):123-126.

Mannschatz T., Pflug B., Borg E., Feger K.H., and Dietrich P. (2014). Uncertainties of LAI estimation from satellite imaging due to atmospheric correction. *Remote Sens. Environ.*, 2014, 153: 24-39. DOI: 10.1016/j.rse.2014.07.020.

Matthews, M.W., Bernard, S., and Winter, K. (2010). Remote sensing of cyanobacteria-dominant algal blooms and water quality parameters in Zeekoevlei, a small hypertrophic lake, using MERIS. *Remote Sens. Environ.*, 114(9), 2070-2087. DOI: 10.1016/j.rse.2010.04.013.

Matthews, M. W., Bernard, S., and Robertson, L. (2012). An algorithm for detecting trophic status, cyanobacterial-dominance, surface scums and floating vegetation in inland and coastal waters. *Remote Sens. Environ.*, 124, 637-652. DOI: 10.1016/j.rse.2012.05. 032.

Miller P I, Shutler J D, Moore G F, and Groom S.B. (2006). SeaWiFS discrimination of harmful algal bloom evolution. *Int. J. Remote Sens.*, 27(11): 2287-2301. DOI: 10.1080/0143116 0500396816.

Oyama, Y., Matsushita, B., and Fukushima, T. (2015). Distinguishing surface cyanobacterial blooms and aquatic macrophytes using Landsat/TM and ETM+ shortwave infrared bands. *Remote Sens. Environ.*, 157, 35-47. DOI: 10.1016/j.rse.2014.04.031.

Pan Y, Shen F, and Verhoef W. (2017). An improved spectral optimization algorithm for atmospheric correction over turbid coastal waters: A case study from the Changjiang (Yangtze) estuary and the adjacent coast. *Remote Sens. Environ.*, 191: 197-214. DOI: 10.1016/j.rse.2017.01.013.

Poggio, L., Gimona, A., and Brown, I. (2012). Spatio-temporal MODIS EVI gap filling under cloud cover: An example in Scotland. *ISPRS journal of photogrammetry and remote sensing*, 72, 56-72. DOI: 10.1016/j.isprsjprs.2012.06.003.

Rhee, G. and Gotham, I. J. (1981). The effect of environmental factors on phytoplankton growth: temperature and the interactions of temperature with nutrient limitation. *Limnol. Oceanogr.*, 26(4), 635-648. DOI: 10.4319/lo.1981.26.4.063 5.

Rotta L.H.S., Alcântara E.H., Watanabe F.S.Y., Rodrigues T.W.P., and Imai N.N. (2016). Atmospheric correction assessment of SPOT-6 image and its influence on models to estimate water column transparency in tropical reservoir. *Remote Sens. Appl.: Soc. and Environ.*, 4: 158-166. DOI: 10.1016/j.rsase.2016.09. 001.

Roy, D. P., Ju, J., Lewis, P., Schaaf, C., Gao, F., Hansen, M., and Lindquist, E. (2008). Multi-temporal MODIS–Landsat data fusion for relative radiometric normalization, gap filling, and prediction of Landsat data. *Remote Sens. Environ.*, 112(6), 3112-3130. DOI: 10.1016/j.rse.2008.03.009.

Sellner, K. G. (1997). Physiology, ecology, and toxic properties of marine cyanobacteria blooms. *Limnol. Oceanogr.*, 42(5), 1089-1104. DOI: 10.4319/lo.1997.42.5_part_2.1089.

Shanmugam, P., Ahn, Y H., and Ram, P.S. (2008). SeaWiFS sensing of hazardous algal blooms and their underlying mechanisms in shelf-slope waters of the Northwest Pacific during summer *Remote Sens. Environ.*, 112(7), 3248-3270. DOI: 10.1016/j.rse.2008.04.002.

Shi K., Zhang Y.,Xu H., Zhu G., Qin B., Huang C.,Liu X.,Zhou Y., and Lv H. (2015). Long-term satellite observations of microcystin concentrations in Lake Taihu during cyanobacterial bloom periods. *Environ. Sci. Technol.*, 49(11), 6448-6456. DOI: 10.1021/es50590 1a.

Shi K., Zhang Y., Zhou Y., Liu X., Zhu G., Qin B., and Gao G. (2017). Long-term MODIS observations of cyanobacterial dynamics in Lake Taihu: Responses to nutrient enrichment and meteorological

factors. *Sci. Rep.*, 7, DOI: 10.1038/srep40326.

Siswanto, E., Ishizaka, J., Tripathy, S.C., and Miyamura, K. (2013). Detection of harmful algal blooms of Karenia mikimotoi using MODIS measurements: A case study of Seto-Inland Sea, Japan. *Remote Sens. Environ.*, 129, 185-196. DOI: 10.1016/j.rse.2012.11.003.

Smayda, T.J. and Trainer, V.L. (2010). Dinoflagellate blooms in upwelling systems: Seeding, variability, and contrasts with diatom bloom behaviour. *Prog. Oceanogr.*, 85(1), 92-107. DOI: 10.1016/j.pocean.2010.02.006.

Song, K., Li, L., Tedesco, L. P., Li, S., Clercin, N. A., Hall, B. E., and Shi, K. (2012). Hyperspectral determination of eutrophication for a water supply source via genetic algorithm–partial least squares (GA–PLS) modeling. *Sci. Total Environ.*, 426, 220-232. DOI: 10.1016/j.scitotenv.20 12.03.058.

Song K.S., Li L., Tedesco L.P., Li S., Clercin N.A., Hall B.E., Li Z.C., and Shi K. (2012). Hyperspectral determination of eutrophication for a water supply source via genetic algorithm–partial least squares (GA–PLS) modeling. *Sci. Total Environ.*, 426, 220-232. DOI: 10.1016/j.scitotenv. 2012.03.058.

Song N., Wang N., Lu Y., and Zhang J.R. (2016). Temporal and spatial characteristics of harmful algal blooms in the Bohai Sea during 1952–2014. *Cont. Shelf Res.*, 122, 77-84. DOI: 10.1016/j.csr.2016.04.006.

Stumpf R.P. and Tomlinson M.C. (2005). Remote sensing of harmful algal blooms. *Remote Sens. Coast. Aquat. Environ.*, 277-296, DOI: 10.1007/978-1-4020-3100-7_12.

Subramaniam, A., Brown, C.W., Hood, R.R., Carpenter, E.J., and Capone, D.G. (2001). Detecting Trichodesmium blooms in SeaWiFS imagery. *Deep Sea Res. (II Top. Stud. Oceanogr.)*, 49(1), 107-121. DOI: 10.1016/S0967-0645(01)00096-0

Vermote, E.F., Tanré, D., Deuze, J.L., Herman, M., and Morcette, J.J. (1997). Second simulation of the satellite signal in the solar spectrum, 6S: An overview. *IEEE Trans. Geosci. Remote Sens.*, 35(3), 675-686. DOI: 10.1109/36.581987

Walsby, A.E., Hayes, P.K., Boje, R., and Stal, L.J. (1997). The selective advantage of buoyancy provided by gas vesicles for planktonic cyanobacteria in the Baltic Sea. *New Phytol.*, 136(3), 407-417. DOI: https://doi.org/10.1046/j.1469-8137.1997.00754.x